Applied Physics B (2018) 124:51
https://doi.org/10.1007/s00340-018-6916-y

Applied Physics B
Lasers and Optics

Interband cascade laser-based ppbv-level mid-infrared methane detection using two digital lock-in amplifier schemes

Fang Song[1] · Chuantao Zheng[1,2] · Di Yu[1] · Yanwen Zhou[1] · Wanhong Yan[1] · Weilin Ye[2,3] · Yu Zhang[1] · Yiding Wang[1] · Frank K. Tittel[2]

Received: 7 January 2018 / Accepted: 13 February 2018

Abstract
A parts-per-billion in volume (ppbv) level mid-infrared methane (CH_4) sensor system was demonstrated using second-harmonic wavelength modulation spectroscopy (2*f*-WMS). A 3291 nm interband cascade laser (ICL) and a multi-pass gas cell (MPGC) with a 16 m optical path length were adopted in the reported sensor system. Two digital lock-in amplifier (DLIA) schemes, a digital signal processor (DSP)-based DLIA and a LabVIEW-based DLIA, were used for harmonic signal extraction. A limit of detection (LoD) of ~ 13.07 ppbv with an averaging time of 2 s was achieved using the DSP-based DLIA and a LoD of ~ 5.84 ppbv was obtained using the LabVIEW-based DLIA with the same averaging time. A rise time of 0→2 parts-per-million in volume (ppmv) and fall time of 2→0 ppmv were observed. Outdoor atmospheric CH_4 concentration measurements were carried out to evaluate the sensor performance using the two DLIA schemes.

1 Introduction

Methane (CH_4) is the second anthropogenic greenhouse gas after carbon dioxide (CO_2) and the increased emission of CH_4 will cause further warming and a continuous change of the global climate system [1]. According to the World Metrology Organization (WMO), Greenhouse Gas Bulletin, the globally atmospheric CH_4 concentration reached a new level of 1853 ± 2 parts-per-billion in volume (ppbv) in 2016, which is ~ 2.6 times of the pre-industrial level (~ 722 ppbv) [2]. Furthermore, compressed natural gas (CNG) is widely used in daily life (e.g., cooking and automotive fuel) and this CNG leakage leads to a further increase of global atmospheric CH_4 concentration levels [3, 4]. In addition, monitoring of CH_4 is useful in studying the carbon cycle and analyzing the sources and sinks of CH_4 [5]. Consequently, measurements and quantification of CH_4 with high accuracy, fast response, and a low limit of detection (LoD) are required.

By targeting an absorption line using a single-mode semiconductor laser, a trace gas species can be detected selectively in real time with high detection sensitivity using tunable laser absorption spectroscopy (TLAS). TLAS is an effective method for CH_4 detection [6, 7]. TLAS and wavelength modulation spectroscopy (WMS) decrease background noise and improve the signal-to-noise ratio (SNR) by encoding and detecting the absorption signal at a high frequency [8–13]. The WMS technique measures CH_4 absorbance with fast response and provides parts-per-million in volume (ppmv) to ppbv detection limits [6, 14], depending on the spectroscopic properties of the target gas and the optical path length. In this work, a WMS-based sensor for atmospheric CH_4 detection was developed using a continuous-wave (CW) interband cascade laser (ICL) operating at ~ 3.291 μm and a 16 m multi-pass gas cell (MPGC) (physical size: $45 \times 11 \times 11$ cm^3, Egold Technology, Wuhan, China) was employed to enhance the CH_4 absorption.

An important step in WMS is the extraction of the harmonic components from the absorbance signal, which was performed by a commercially available lock-in amplifier (model SR830, Stanford Research System, USA) [15, 16]

This article is part of the topical collection "Mid-infrared and THz Laser Sources and Applications" guest edited by Wei Ren, Paolo De Natale and Gerard Wysocki.

✉ Chuantao Zheng
zhengchuantao@jlu.edu.cn

[1] State Key Laboratory of Integrated Optoelectronics, College of Electronic Science and Engineering, Jilin University, 2699 Qianjin Street, Changchun 130012, China

[2] Department of Electrical and Computer Engineering, Rice University, 6100 Main Street, Houston, TX 77005, USA

[3] College of Engineering, Shantou University, 243 Daxue Road, Shantou 515063, China

Published online: 23 February 2018

and a LabVIEW-based digital lock-in amplifier (DLIA) [17–19]. However, due to the large size and high power consumption, these two lock-in amplifiers are more suitable for laboratory measurements. Targeting mobile and field gas measurements (e.g., in mining safety operation and mobile atmospheric gas measurements), there is demand in terms of size, power consumption, and reliability for infrared gas sensor systems, which requires miniaturization of both optical and electrical sub-systems. For example, when targeting field applications using compact electronics and a small-sized gas cell, several portable CH_4 sensor systems have been developed using non-dispersive infrared (NDIR) [20] and near-infrared TLAS techniques [21]. Compared to our previously reported LabVIEW-based DLIA platforms for WMS-based CH_4 and ethane (C_2H_6) detection [17–19], in this work, a portable, low-power-budget, board-level DLIA is proposed for field application, whose data acquisition and orthogonal lock-in algorithm were realized by a compact digital signal processor (DSP) board. Measurements were performed to determine the sensor sensitivity, precision and response time using the two DLIA schemes. The sensor system performance was also evaluated by means of outdoor atmospheric CH_4 measurements. The measurement results validate the feasibility of the DSP-based miniaturized DLIA as well as laptop-based DLIA.

2 Sensor configuration and design details

2.1 CH_4 absorption line selection

Based on the high-resolution transmission (HITRAN) molecular absorption database [22, 23], the strongest CH_4 absorptions are located in the mid-infrared spectral region at 3.31 μm. Hence, with commercially available, room-temperature laser sources emitting CW radiation in the 3–4 μm range, a wavelength of 3.291 μm is the best choice as the target absorption band for CH_4 detection. The CH_4 absorption line intensity in the range from 3.0 to 3.8 μm is shown in Fig. 1a. The absorption spectra of a mixture consisting of 1.8 ppmv CH_4 and a 2% H_2O are depicted in Fig. 1b, where the pressure is 1 atm and the optical path length is 16 m. The 3038.5 cm^{-1} absorption line was selected as the optimum target line, taking the interference of H_2O on CH_4 detection into consideration. The line strength is 2.195 cm^{-2} atm^{-1}, the air- and self-broadening coefficients are 0.0645 and 0.081 cm^{-1} atm^{-1}, respectively, and the half width at half-maximum (HWHM) is 0.067 cm^{-1} at an operating pressure of 1 atm and a temperature of 296 K.

2.2 Sensor configuration based on two digital lock-in amplifier schemes

The mid-infrared CH_4 sensor structure is shown in Fig. 2, including both the optical and electrical sub-systems. In the optical part, a Nanoplus CW, thermoelectrically cooled (TEC), distributed feedback (DFB) ICL was used as the excitation laser source. A TEC mercury-cadmium-telluride (MCT) photodetector (VIGO System, model PVI-4TE-5) with a detectivity of ~ 1.2×10^{11} $cmHz^{1/2}/W$ was used to

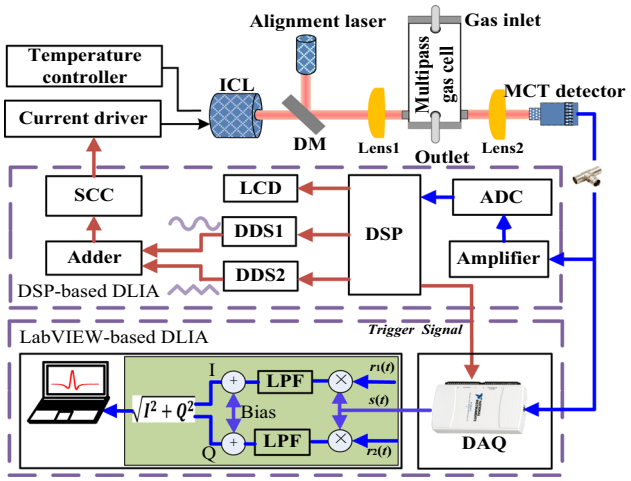

Fig. 2 Schematic of a CH_4 sensor system based on a CW, TEC ICL, where a DSP-based and a LabVIEW-based DLIA were employed for harmonic extraction

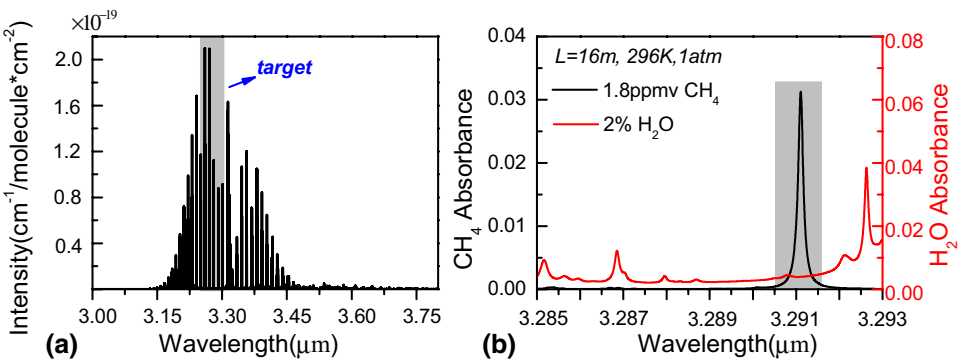

Fig. 1 **a** HITRAN-based absorption spectra of CH_4 from 3.0 to 3.8 μm. **b** HITRAN-based absorption spectra of CH_4 (1.8 ppmv) and H_2O (2%) in a narrow spectral range from 3.285 to 3.293 μm at a pressure of 1 atm and an absorption length of 16 m

measure the output laser power. A dichroic mirror (DM) was used to combine the mid-infrared ICL beam with a visible diode laser beam for achieving optimum optical alignment. The combined beams were directed into the MPGC using a CaF_2 lens (Lens 1, $f = 30$ mm). In the electrical system, an integrated laser current driver (Thorlabs, LDC210C) and a temperature controller (Thorlabs, TED200C) were used to drive the ICL. For the DSP-based DLIA, two direct digital synthesizers (DDSs) are used to generate a scan signal as well as a modulation signal. Processed by an adder and signal conditioning circuit (SCC), the drive signal is sent to the integrated laser current driver. The MCT detector signal was sent to the DSP-based DLIA and the LabVIEW-based DLIA simultaneously for harmonic signal extraction. The LabVIEW-based DLIA was realized based on a data acquisition (DAQ) card (National Instrument, model USB-6211). Finally, the CH_4 concentration levels were determined by means of a laptop computer.

2.3 Design details of the DLIAs

The principle of an orthogonal lock-in amplifier was described in Refs [24, 25]. The input of the DLIA is given by $s(t) = A\sin(\omega t + \theta) + n(t)$, where A is the amplitude of the input signal and $n(t)$ is the signal channel noise. There are two orthogonal reference signals, i.e., $r_1(t) = B\sin(\omega t)$ and $r_2(t) = -B\cos(\omega t)$, where B is the amplitude of the reference signal. Upon multiplication and low-pass filtering, two orthogonal components $I = \frac{AB}{2}\cos\theta$ and $Q = -\frac{AB}{2}\sin\theta$ are obtained to represent the gas concentration.

2.3.1 DSP-based DLIA

The DSP-based orthogonal DLIA is shown in Fig. 3. The DSP was commercially available from Texas Instrument as model TMS320F28335. An analog-to-digital convertor (ADC) module (model # AD7902) was used for data sampling, which consists of a dual pseudo differential 16-bit, 1 MSPS convertor with low-power consumption of ~ 12 mW. After ADC processing, the sampled signal was sent to the DSP for multiplication and filtering by an orthogonal lock-in amplifier algorithm shown in the green region of Fig. 2. The 2*f* signal was extracted and displayed on a liquid crystal display (LCD) screen. To reduce the electrical power consumption, the power tree of the DLIA was optimized for in-situ measurements. The supply currents of the + 12 and − 12 V power rail were measured using a digital multi-meter to be 275 and 26 mA, respectively, resulting in a total power consumption of 3.612 W.

2.3.2 LabVIEW-based DLIA

The schematic of the LabVIEW-based DLIA is shown in Fig. 2. The ADC module of the DAQ card has a resolution of 16 bits and a sampling frequency of 250 k sps (samples per second). The input voltage range of the DAQ is − 10 to + 10 V. After ADC processing, the sampled signal was multiplied by two frequency-doubled, orthogonal signals synchronized by the modulation signal. With low-pass filtering (LPF), biased adding operation (Bias) and square operation, two orthogonal components (I and Q) were obtained. Then, using a second adding operation between the two components and a square root (sqrt) operation, the 2*f* signal was acquired. Without bias, the obtained 2*f* signal is completely above the zero baseline, whose waveform is not the same as that of the commercial lock-in amplifier (e.g. SR830). Upon adding a bias to the two components (I and Q), the baseline of the 2*f* signal is not zero and the obtained 2*f* signal is on both sides of the non-zero baseline. Then, using a baseline fitting and elimination, the baseline becomes zero, and the finally obtained 2*f* signal will be on both sides of the zero baselines, whose waveform is the same as that of the commercial lock-in amplifier (SR830).

2.4 Modulation depth optimization

In the case of simultaneous detection using the DSP-base and LabVIEW-based DLIA, the normalized amplitude of the 2*f* signal was recorded at different modulation amplitudes at a pressure of 1 atm, as depicted in Fig. 4. If the

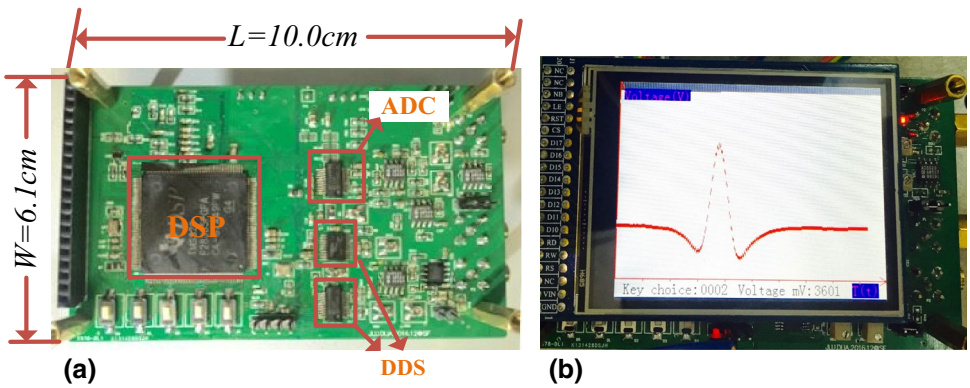

Fig. 3 **a** Photograph of the DSP-based DLIA board. **b** Photograph of the DSP-based DLIA board with a LCD indicating the 2*f* signal

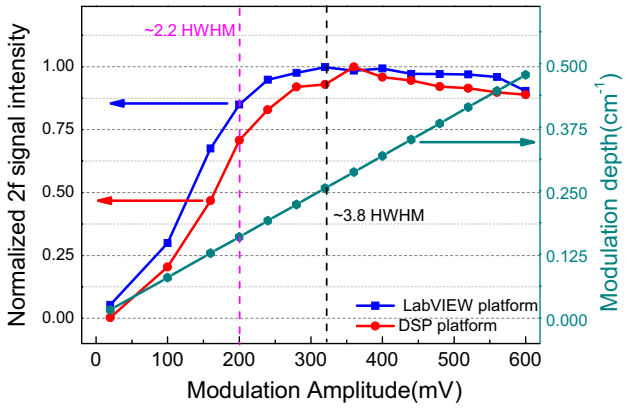

Fig. 4 Normalized 2*f* signal amplitude and modulation depth as a function of modulation amplitude for a 2 ppmv CH_4 sample, where the modulation frequency was 2 kHz

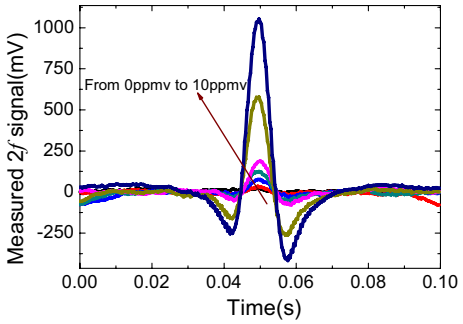

Fig. 5 Measured 2*f* waveforms with the DSP-based DLIA for seven CH_4 concentration levels of 0, 0.2, 0.5, 1, 2, 5, and 10 ppmv, where the balance gas was N_2

modulation coefficient is chosen to have a theoretical value of 2.2 [26, 27], the normalized 2*f* signal amplitude is ~0.7 times of the maximum 2*f* signal. The maximum 2*f* signal of the DSP-based DLIA is achieved at a modulation depth of 0.2549 cm^{-1} leading to a modulation amplitude of ~320 mV. The maximum 2*f* signal of the LabVIEW-based DLIA is achieved at a modulation depth of 0.3187 cm^{-1}, corresponding to a modulation amplitude of ~400 mV. Therefore, the modulation amplitude was set to ~320 mV to enable design consistency of the sensor system for the two DLIA schemes, leading to a modulation coefficient of ~3.8.

3 Sensor performance using a DSP-based DLIA

3.1 Experimental details

The mid-infrared CH_4 sensor system based on the DSP-based DLIA was operated at a drive current and temperature of 52 mA and 15 °C, respectively. The pressure inside the MPGC was set to 1 atm and the gas sample was pumped into the gas cell using an oil-free vacuum pump (KNF Neuberger Inc., model N 813.5 ANE/AF). A triangular scan signal with a frequency of 5 Hz and a peak-to-peak amplitude of 2 V was used. The modulation signal was a sinusoidal signal of 2 kHz with an optimized amplitude of 320 mV. The sampling rate of the 16 bit ADC module was set to 80 kHz. By averaging the sampled absorption data in each modulation period, one 2*f* spectral point was obtained. Therefore, each triangular period (including two CH_4 absorption spectra) contains 400 data points for a 2*f* signal. Data sampling was triggered by a synchronized signal from the DSP to realize synchronization with the scan signal. The extracted 2*f* signal was displayed on the LCD screen and sent to the laptop by a USB port for post data analysis. The dynamic current was measured using a digital multi-meter for power consumption evaluation of the DSP-based DLIA. CH_4 sensor calibration was carried out using diluted standard CH_4 gas samples with seven concentration levels of 0, 0.2, 0.5, 1, 2, 5, and 10 ppmv. Furthermore, the LoD and dynamic response of the DSP-based DLIA sensor system are used to demonstrate the sensor performance.

3.2 Results and discussion

Using nitrogen (N_2) as the balance gas, CH_4 samples with different concentration levels from 0 to 10 ppmv were prepared. The obtained 2*f* waveforms are shown in Fig. 5. The amplitude of the 2*f* signal, defined by $\max[A_{2f}(t)]$, increases as the concentration level increases due to the larger absorption at the peak absorption wavelength. The calibration was carried out by pumping different gas samples into the MPGC and measuring the amplitude of the 2*f* signal. Each sample was tested for ~6 min. The measured data of $\max[A_{2f}(t)]$ for each concentration were averaged and plotted as a function of CH_4 concentration, as shown in Fig. 6a. A linear relation between $\max[A_{2f}(t)]$ and C was shown in Fig. 6b. The fitting curve is given by:

$$C = 0.00949 \times \max[A_{2f}(t)] - 0.19927, \quad (1)$$

where C is in ppmv and $\max[A_{2f}(t)]$ is in mV. The fitting curve indicates a good linear relationship (R^2 99.64%) between $\max[A_{2f}(t)]$ and C. Equation (1) was used to determine the CH_4 concentration levels based on the measured amplitude of the 2*f* absorbance signal.

A long-term stability and precision of the CH_4 sensor were measured by monitoring a 0 ppmv CH_4 sample (pure N_2) for ~2 h. Figure 7a exhibits the measured concentration versus time t and Fig. 7b shows the Allan–Werle deviation as a function of the averaging time τ. The Allan deviation is ~13.07 ppbv for a 2 s averaging time and shows an optimum averaging time of 516 s corresponding to a minimum

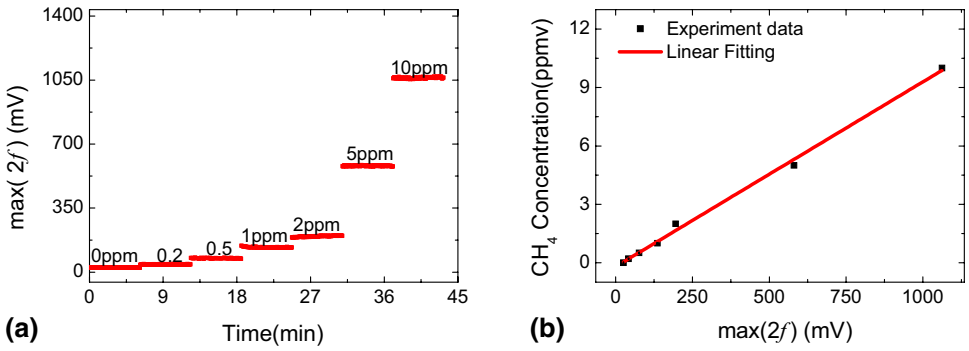

Fig. 6 **a** Measured max[$A_{2f}(t)$] (mV) as a function of the calibration time t with the DSP-based DLIA for seven CH_4 concentration levels of 0, 0.2, 0.5, 1, 2, 5, and 10 ppmv. **b** Experimental data dots and fitting curve of CH_4 concentration as a function of max[$A_{2f}(t)$] (mV)

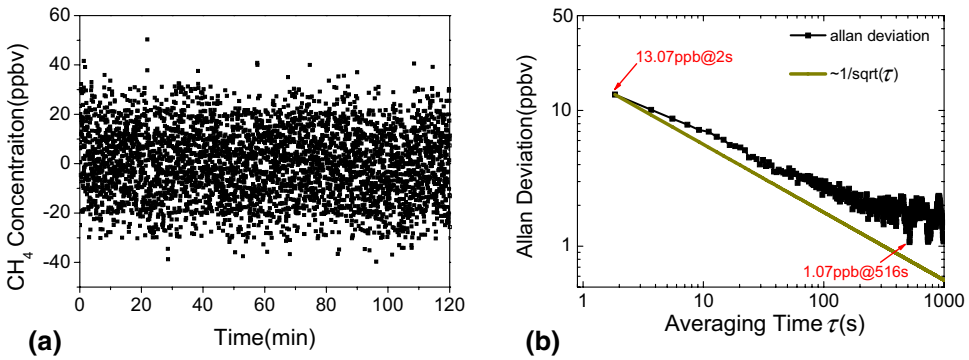

Fig. 7 **a** Measured concentration using the DSP-based DLIA with pure N_2 inside the MPGC to establish the zero background CH_4 concentration condition. **b** Allan–Werle deviation plot as a function of averaging time, τ, based on the data shown in (**a**)

detection sensitivity of ~ 1.07 ppbv. At short averaging times, the sensor was mainly dominated by White-Gaussian noise. The Allan deviation decreases by increasing the averaging time, which is proportional to sqrt ($1/\tau$) shown by the dark yellow solid line. However, at long averaging time, sensor drift starts to occur and the Allan deviation increases.

A 'Y' gas connector with two entrance ports and one exit port was used to illustrate the dynamic response of the DSP-based DLIA sensor. One of the entrance ports was connected to a pure N_2 cylinder and the other one was connected to a standard 2 ppmv CH_4 cylinder. Two needle valves were used at the two entrance ports to switch the two input cylinders either to "on" or "off". The exit port was connected to the MPGC. The test result is shown in Fig. 8. With a gas flow rate of ~ 500 mL min^{-1}, a 10–90% rise time of ~ 22–35 s was obtained for the two concentration changes. Then, with pure N_2 as the diluting gas, the mass flow controller (MFC) was set to "Purge". In this case, a 90–10% fall time of 7 s (in the insert in Fig. 8) was determined by means of the gas purge operation.

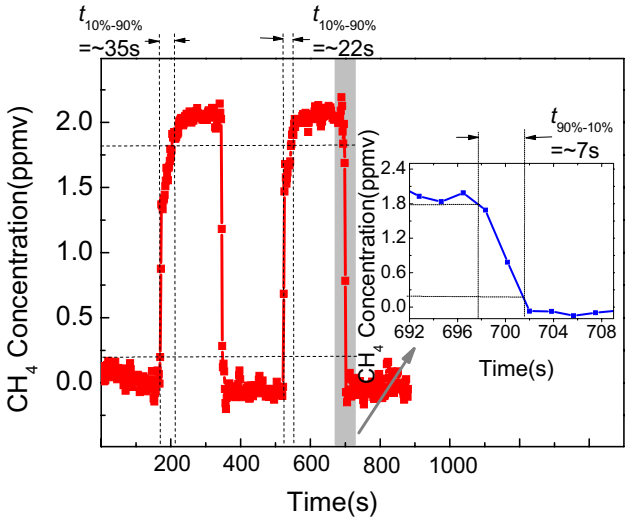

Fig. 8 Dynamic response by varying CH_4 concentration between 0 and 2 ppmv with the DSP-based DLIA platform. Rise time: pumping of a standard 2 ppmv CH_4 sample into the MPGC with a gas flow rate of 500 mL min^{-1}; Fall time: the MFC was set to "Purge" for pumping pure N_2 into the MPGC

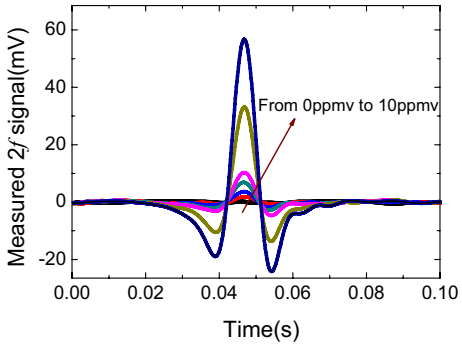

Fig. 9 Measured 2*f* waveforms with the LabVIEW-based DLIA for seven CH_4 concentration levels of 0, 0.2, 0.5, 1, 2, 5, and 10 ppmv, where the balance gas was N_2

4 Sensor performances using the LabVIEW-based DLIA

4.1 Experimental details

The ICL driver current, laser temperature, and the pressure in the MPGC were the same as those used in the DSP-based DLIA scheme. The LabVIEW-based DLIA platform shares the same scan and modulation signal from the DSP-based DLIA board. The sampling rate of the DAQ card was set to 200 kHz. As a result, each triangular period (5 Hz) contains 40,000 data points. Data sampling was triggered by a synchronized trigger signal from the DSP board, as depicted in Fig. 2. The data of max[$A_{2f}(t)$] were recorded by a laptop for subsequent processing and analyzing. To compare with the DSP-based DLIA scheme, the LabVIEW-based DLIA CH_4 sensor calibration was carried out using the same diluted standard CH_4 gas samples as those described in the previous Sect. 3.

4.2 Results and discussion

Figure 9 shows the measured 2*f* waveforms for seven different CH_4 concentration levels 0, 0.2, 0.5, 1, 2, 5, and 10 ppmv. Figure 10a shows a time series of the 2*f* signal amplitude measurements at the seven different CH_4 concentrations. For each CH_4 concentration level, a measurement lasting ~ 6 min was taken. The measured 2*f* signal amplitudes for each concentration were averaged and plotted in Fig. 10b. A linear relation is found between them, which is represented by the following fitting curve as:

$$C = 0.17793 \times \max[A_{2f}(t)] - 0.1681, \quad (2)$$

where *C* is in ppmv and max[$A_{2f}(t)$] is in mV. The CH_4 concentration can be determined by max[$A_{2f}(t)$]. The fitting curve indicates a good linear relationship with an R^2 value of 99.92%.

A CH_4 concentration measurement of the sample with zero concentration (pure N_2) was performed for a time period of ~ 2 h using the LabVIEW-based DLIA. The total

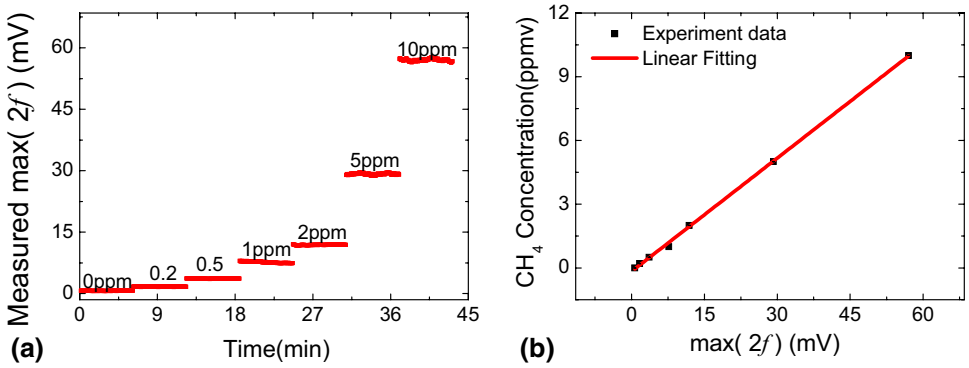

Fig. 10 **a** Measured max[A_{2f}(t)] (mV) versus calibration time *t* with the LabVIEW-based DLIA for seven CH_4 concentration levels of 0, 0.2, 0.5, 1, 2, 5, and 10 ppmv. **b** Experimental data dots and fitting curve of CH_4 concentration versus max[$A_{2f}(t)$] (mV)

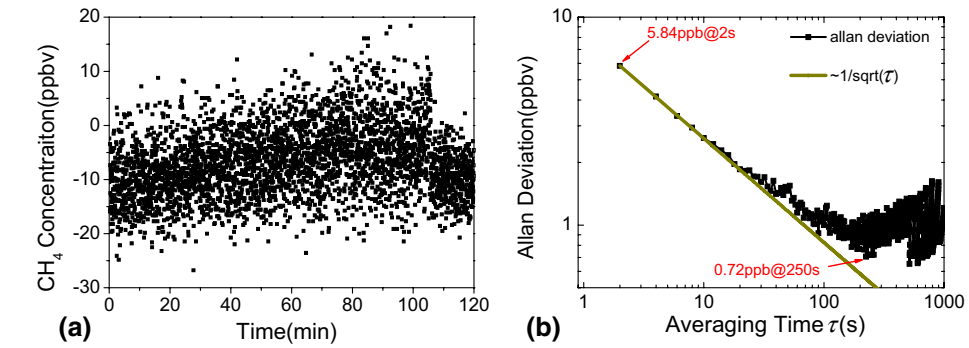

Fig. 11 **a** Measured concentration using the LabVIEW-based DLIA by pumping pure N_2 into the MPGC to establish the zero background CH_4 concentration condition. **b** Allan–Werle deviation plot as a function of averaging time, τ, based on the data shown in **a**

variation range of the measured concentration is ~ ± 27 ppbv for an observation time of ~ 120 min, as shown in Fig. 11a. Allan–Werle deviation was plotted on a log–log scale versus the averaging time, τ, as shown in Fig. 11b. The plot indicates a measurement precision of ~ 5.84 ppbv with a 2 s averaging time. The Allan–Werle plot shows an optimum averaging time of ~ 250 s, corresponding to a precision of ~ 0.72 ppbv. However, as the averaging time continues to increase, the Allan–Werle deviation increases again, which shows that sensor system drift becomes a dominant factor and decreases the sensor stability. The dark yellow solid line, which is proportional to sqrt($1/\tau$), indicates that the theoretically expected behavior of the sensor system is a White-Gaussian noise dominated region prior to when sensor system drifts start to occur.

The dynamic performance of the LabVIEW-based DLIA sensor was measured, as shown in Fig. 12. The measurement procedure was the same as that used in Sect. 3.2. Dynamic measurements of the sensor system indicate a 10–90% rise time of ~ 30 to 40 s and a 90–10% fall time of ~ 6 s under a "Purge" operation, which are almost the same as when compared with the DSP-based DLIA system.

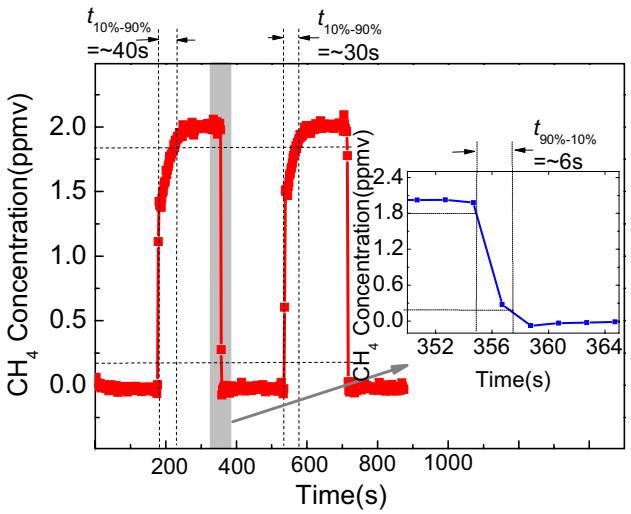

Fig. 12 Dynamic response by varying CH_4 concentration between 0 and 2 ppmv with the LabVIEW-based DLIA. Rise: pumping a standard 2 ppmv CH_4 sample into the MPGC with a gas flow rate of 500 mL min^{-1}; Fall: the MFC was set to "Purge" pumping pure N_2 into the MPGC

5 Comparison and atmospheric CH_4 measurements

5.1 Inter-comparison of the two DLIA schemes

Atmospheric CH_4 concentration measurements were realized using the two lock-in schemes and the same optical part. The performance comparison of the two sensor systems is listed in Table 1. The DSP-based DLIA for CH_4 concentration measurements is easy to use due to its compact size and low-power consumption. The LabVIEW-based DLIA technique, which requires a laptop to perform signal processing, is more complex and costly than the DSP-based DLIA method. However, because of a high sampling rate and effective data processing ability, the sensor will be more sensitive using the LabVIEW-based DLIA. A similar response behavior was found for the two schemes, with a rise time of ~ 30 s and a fall time of < 10 s for the gas test conditions. Hence, the two detection schemes can be applied in different applications, depending upon the requirement of the sensor system performance.

5.2 Comparison with other reported CH_4 sensor systems

As a comparison, the performances of several reported CH_4 sensor systems based on WMS technique and different infrared lasers (mid-infrared quantum cascade laser (QCL), mid-infrared ICL and near-infrared distributed feedback diode laser (DFB-DL)) are listed in Table 2. Various DLIAs were used in the sensor systems, involving the commercial products (Signal Recovery 7265, Stanford SR830), the LabVIEW platform on a laptop, as well as compact board-level electronics. Compared with the systems based on commercial and laptop DLIA, the proposed sensor system using a board-level DLIA possesses a similar ppbv-level high detection sensitivity but with a reduced sensor size, power consumption, and cost.

5.3 Atmospheric CH_4 measurements

The performance of the CH_4 sensor system based on the two DLIA schemes was evaluated by performing atmospheric CH_4 concentration measurements. Using a sample line, the

Table 1 Inter-comparison of the CH_4 sensor system performance obtained with two different DLIA schemes

DLIA scheme	Allan deviation	Response time	Power consumption (W)	Size
DSP-based	13.1 ppbv (@ 2 s) 1.1 ppbv (@ 516 s)	Rise ~ 30 s Fall ~ < 10 s	3.6	10.0 × 6.1 × 3.0 cm^3
LabVIEW-based	5.8 ppbv (@ 2 s) 0.7 ppbv (@ 250 s)	Rise ~ 30 s Fall ~ < 10 s	45.3	16.9 × 9.4 × 3.1 cm^3 + a laptop

Table 2 Performance comparison of three reported CH_4 sensor systems and the reported sensor system

Refs.	Wavelength (μm)	Laser source	Path length (m)	Allan deviation	DLIA type
Ren et al. [28]	7.8	QCL	57.6	5.9 ppb (@ 1 s)	Commercial (Signal Recovery 7265)
Ye et al. [18]	3.337	ICL	54.6	11.2 ppb (@ 3.4 s)	Laptop (LabVIEW)
Liu et al. [29]	1.653	DFB-DL	26.4	79 ppb (@ 1 s)	Commercial (SR830)
Reported sensor	3.291	ICL	16	13.1 ppb (@2 s)	Compact electronics (DSP board)
				5.8 ppb (@2 s)	Laptop (LabVIEW)

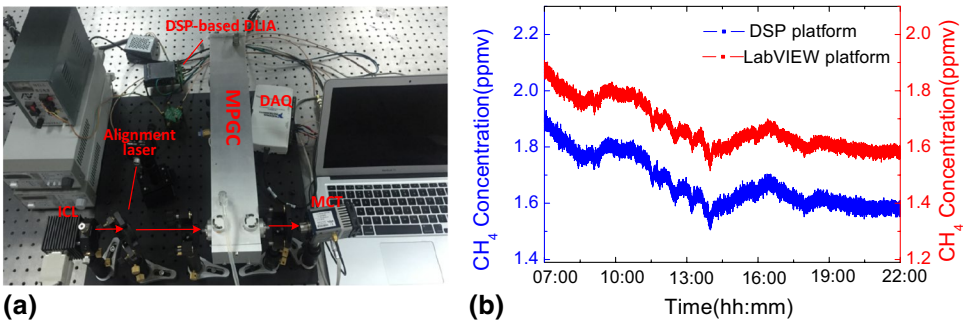

Fig. 13 **a** Photograph of the sensor system for CH_4 measurements. **b** Measurement results of CH_4 monitoring in the atmosphere for a ~ 15 h duration on the Jilin University Campus, Changchun, China. The red curve is the measured concentration with the LabVIEW-based DLIA and the blue curve is the measured concentration using the DSP-based DLIA

outdoor air was pumped into the MPGC and continuous outdoor CH_4 concentration measurements were conducted. A photograph of the two DLIA platforms is shown in Fig. 13a and the measured concentrations are plotted in Fig. 13b. Fluctuations in the CH_4 concentration levels were observed during ~ 15 h atmospheric monitoring of CH_4. When using the DSP-based DLIA, the measured concentrations show an average value of ~ 1.670 ppmv ± 88.8 ppbv (1σ). In comparison, an average value of ~ 1.671 ppmv ± 83.7 ppbv (1σ) was obtained with the LabVIEW-based DLIA. The measurement results verified that the reported sensor system can be used effectively to monitor atmospheric CH_4 concentration levels.

6 Conclusions

A CW, TEC, DFB ICL-based ppbv-level mid-infrared sensor was developed for atmospheric CH_4 detection using a CH_4 absorption line located at 3038.5 cm^{-1} and a MPGC with a 16 m optical path length. Two signal processing schemes, a DSP-based DLIA and a LabVIEW-based DLIA, were employed to assess the CH_4 sensor performance. The sensor shows a measurement precision of ~ 13.07 and ~ 5.84 ppbv with a ~ 2 s averaging time, respectively, when using the DSP-based and the LabVIEW-based DLIA, Dynamic measurements of the two schemes were carried out. Outdoor atmospheric CH_4 measurements were conducted to evaluate the long-term sensor performance. Compared to the LabVIEW-based DLIA scheme, the DSP-based DLIA shows the merits of compact size, low cost, and low-power consumption, which is suitable for portable infrared gas sensing applications.

Acknowledgements The National Natural Science Foundation of China (Nos. 61627823, 61775079), National Key R&D Program of China (Nos. 2017YFB0402800, 2016YFD0700101, 2016YFC0303902), Key Science and Technology R&D program of Jilin Province, China (No. 20180201046GX), Industrial Innovation Program of Jilin Province, China (No. 2017C027), and the National Science Foundation (NSF) ERC MIRTHE award and Robert Welch Foundation (No. R4925U).

References

1. R.K. Pachauri, M. Allen, V. Barros, J. Broome, W. Cramer, R. Christ, J. Church, L. Clarke, Q. Dahe, P. Dasgupta, Climate change 2014: synthesis report: contribution of working groups I, II and III to the fifth assessment report of the intergovernmental panel on climate change. J. Roman. Stud. **4**(2), 85–88 (2015)
2. World Metrological Organization, The state of greenhouse gases in the atmosphere based on global observations through 2016. WMO-GAW Greenh. Gas Bul. **13**, 1–8 (2017)
3. A.R. Brandt, G.A. Heath, E.A. Kort, F. O'Sullivan, G. Pétron, S.M. Jordaan, R. Harriss, Energy and environment: methane leaks from North American natural gas systems. Science **343**(6172), 733–735 (2014)
4. R.A. Alvarez, S.W. Pacala, J.J. Winebrake, W.L. Chameides, S.P. Hamburg, Greater focus needed on methane leakage from natural gas infrastructure. Proc. Natl. Acad. Sci. USA **109**(17), 6435–6440 (2012)
5. E.S.F. Berman, M. Fladeland, J. Liem, R. Kolyer, M.Gupta, Greenhouse gas analyzer for measurements of carbon dioxide, methane, and water vapor aboard an unmanned aerial vehicle. Sens. Actuators B **169**(4), 128–135 (2012)
6. Y. Cao, N.P. Sanchez, W. Jiang, R.J. Griffin, F. Xie, L.C. Hughes, C. Zah, F.K. Tittel, Simultaneous atmospheric nitrous oxide,

methane and water vapor detection with a single continuous wave quantum cascade laser. Opt. Express. **23**(3), 2121–2132 (2015)
7. Y. Yu, N.P. Sanchez, R. J.Griffin, F. K.Tittel, CW EC-QCL-based sensor for simultaneous detection of H_2O, HDO, N_2O and CH_4 using multi-pass absorption spectroscopy. Opt. Express. **24**(10), 10391–10401 (2016)
8. C.S. Goldenstein, I.A. Schultz, R.M. Spearrin, J.B. Jeffries, R.K. Hanson, Scanned wavelength modulation spectroscopy near 2.5 μm for H_2O and temperature in a hydrocarbon-fueled scramjet combustor. Appl. Phys. B **116**(3), 717–727 (2014)
9. C.S. Goldenstein, R.M. Spearrin, R.K. Hanson, Fiber-coupled diode-laser sensors for calibration-free stand-off measurements of gas temperature, pressure, and composition. Appl. Opt. **55**(3), 479–484 (2016)
10. L.C. Philippe, R.K. Hanson, Laser diode wavelength-modulation spectroscopy for simultaneous measurement of temperature, pressure, and velocity in shock-heated oxygen flows. Appl. Opt. **32**(30), 6090–6103 (1993)
11. J.T. Liu, G.B. Rieker, J.B. Jeffries, M.R. Gruber, C.D. Carter, T. Mathur, Near-infrared diode laser absorption diagnostic for temperature and water vapor in a scramjet combustor. Appl. Opt. **44**(31), 6702–6711 (2005)
12. K. Sun, X. Chao, R. Sur, C.S. Goldenstein, J.B. Jeffries, R.K. Hanson, Analysis of calibration-free wavelength-scanned wavelength modulation spectroscopy for practical gas sensing using tunable diode lasers. Meas. Sci. Technol. **24**(12), 1–12 (2013)
13. G.B. Rieker, J.B. Jeffries, R.K. Hanson, Calibration-free wavelength-modulation spectroscopy for measurements of gas temperature and concentration in harsh environments. Appl. Opt. **48**(29), 5546–5560 (2009)
14. R. Sur, K. Sun, J.B. Jeffries, J.G. Socha, R.K. Hanson, Scanned-wavelength-modulation-spectroscopy sensor for CO, CO_2, CH_4, and H_2O in a high-pressure engineering-scale transport-reactor coal gasifier. Fuel **150**, 102–111 (2015)
15. L. Dong, W.G. Ma, W.B. Yin, C.Y. Li, S.T. Jia, Experimental study on harmonic detection of methane by use of a digital lock-in amplifier. Spectrosc. Spectr. Anal. **25**(3), 473–476 (2005)
16. L. Dong, Y.J. Yu, C.G. Li, S. So, F.K. Tittel, Ppb-level formaldehyde detection using a cw room-temperature interband cascade laser and a miniature dense pattern multipass gas cell. Opt. Express. **23**(15), 19821 (2015)
17. C.T. Zheng, W.L. Ye, N.P. Sanchez, A.K. Gluszek, A.J. Hudzikowski, C.G. Li, L. Dong, J.G. Robert, F.K. Tittel, Infrared dual-gas CH_4/C_2H_6 sensor using two continuous-wave interband cascade lasers. IEEE Photonics Technol. Lett. **28**(21), 2351–2354 (2016)
18. W.L. Ye, C.G. Li, C.T. Zheng, N.P. Sanchez, A.K. Gluszek, A.J. Hudzikowski, L. Dong, R.J. Griffin, F.K. Tittel, Mid-infrared dual-gas sensor for simultaneous detection of methane and ethane using a single continuous-wave interband cascade laser. Opt. Express. **24**(15), 16973–16985 (2016)
19. C.G. Li, C.T. Zheng, L. Dong, W.L. Ye, F.K. Tittel, Y.D. Wang, Ppb-level mid-infrared ethane detection based on three measurement schemes using a 3.34-μm continuous-wave interband cascade laser. Appl. Phys. B **122**(7), 185 (2016)
20. C.T. Zheng, W.L. Ye, G.L. Li, X. Yu, C.X. Zhao, Z.W. Song, Y.D. Wang, Performance enhancement of a mid-infrared CH_4 detection sensor by optimizing an asymmetric ellipsoid gas-cell and reducing voltage-fluctuation: theory, design and experiment. Sens. Actuators B **160**(1), 389–398 (2011)
21. B. Li, C.T. Zheng, H.F. Liu, Q.X. He, W.L. Ye, Y. Zhang, J.Q. Pan, Y.D. Wang, Development and measurement of a near-infrared CH_4 detection system using 1.654 μm wavelength-modulated diode laser and open reflective gas sensing probe. Sens. Actuators B **225**, 188–198 (2016)
22. L.S. Rothman, I.E. Gordon, Y. Babikov, A. Barbe, D.C. Benner, P.F. Bernath, M. Birk, L. Bizzocchi, V. Boudon, L.R. Brown, A. Campargue, K. Chance, E.A. Cohen, L.H. Coudert, V.M. Devi, B.J. Drouin, A. Fayt, J.M. Flaud, R.R. Gamache, J.J. Harrison, J.M. Hartmann, C. Hill, J.T. Hodges, D. Jacquemart, A. Jolly, J. Lamouroux, R.J. Le Roy, G. Li, D.A. Long, O.M. Lyulin, C.J. Mackie, S.T. Massie, S. Mikhailenko, H.S.P. Müller, O.V. Naumenko, A.V. Nikitin, J. Orphalu, V. Perevalov, A. Perrin, E.R. Polovtseva, C. Richard, M.A.H. Smith, E. Starikova, K. Sung, S. Tashkun, J. Tennyson, G.C. Toon, V.G. Tyuterev, G. Wagner, The Hitran 2012 molecular spectroscopic database. J. Quant. Spectrosc. Radiat. Transf. **130**, 4–50 (2013)
23. H.I.T.R.A.N. The Database, https://www.cfa.harvard.edu/hitran/. Accessed 30 Oct 2017
24. A. Chighine, E. Fisher, D. Wilson, M. Lengden, W. Johnstone, H. Mccann, An FPGA-based lock-in detection system to enable chemical species tomography using TDLAS. IEEE International Conference on Imaging Systems and Techniques, pp. 1–5 (2015)
25. H.F. Liu, B. Li, Q.X. He, J.M. Dang, H.Y. Yu, C.T. Zheng, Y.D. Wang, Development of a digital orthogonal lock-in amplifier and its application in methane detection. Acta Photon. Sin. **45**(4), 18–23 (2016) (**Chinese**)
26. K. Liu, T. Liu, J. Jiang, G.D. Peng, H. Zhang, D. Jia, Y. Wang, W. Jing, Y. Zhang, Investigation of wavelength modulation and wavelength sweep techniques in intracavity fiber laser for gas detection. J. Lightwave Technol. **29**(1), 15–21 (2011)
27. J. Reid, D. Labrie, Second-harmonic detection with tunable diode lasers-comparison of experiment and theory. Appl. Phys. B **26**(3), 203–210 (1981)
28. W. Ren, W.Z. Jiang, F.K. Tittel, Single-QCL-based absorption sensor for simultaneous trace-gas detection of CH_4 and N_2O. Appl. Phys. B **117**(1), 245–251 (2014)
29. K. Liu, L. Wang, T. Tan, G.S. Wang, W.J. Zhang, W.D. Chen, X.M. Gao, Highly sensitive detection of methane by near-infrared laser absorption spectroscopy using a compact dense-pattern multipass cell. Sens. Actuators B **220**, 1000–1005 (2015)